Blackberry Structures

DOI: 10.1002/anie.201007829

Viral-Capsid-Type Vesicle-Like Structures Assembled from $M_{12}L_{24}$ Metal–Organic Hybrid Nanocages**

Dong Li, Wu Zhou, Kai Landskron, Sota Sato, Christopher J. Kiely, Makoto Fujita, and Tianbo Liu**

Viral capsids contain multiple copies of identical monomer or dimer proteins arranged into monolayered spherical structures with icosahedral symmetry. These spherical structures (capsids) can wrap up the genome. For example, the capsids of wild hepatitis B virus (HBV) have a diameter of approximately 20 nm and contain 120 copies of a dimer protein.[1] The viral capsid proteins can also assemble into vesicles in vitro under appropriate conditions (e.g. high ionic strength, low pH value) without the viral genome. The hydrophobic interactions, hydrogen bonding, and electrostatic interactions between capsid monomers/dimers are important for the process.[1,2] For a better understanding of the complex nature of viral-capsid formation, and the breathing and swelling modes of the virus, simple analogous model systems are needed to mimic the self-assembly process of viral capsids.[3] Although hydrophobic interactions are generally believed to be the major driving force for the construction of viral capsids, they cannot explain some phenomena, such as the salt effect.[1,4] On the other hand, underestimated electrostatic interactions might play a role, as the proteins are charged macroions. One important factor which may reflect the nature of attractive interactions is the interparticle distance between the building blocks on the surface of the assembled structures. However, this crucial information is usually difficult to obtain.

Recent studies have shown that hydrophilic macroions with sizes between those of simple ions and large colloids behave completely differently from smaller and larger macroions. Both macroanions (including various polyoxometalates, or POMs) and macrocations (such as metal–organic nanocages) slowly assemble into single-layered, spherical, vesicle-like "blackberry" structures in polar solvents.[5] However, a major difference between metal–organic nanocages and POMs is that the former entities contain multiple hydrophobic domains, which might affect the self-assembly process by introducing additional driving forces. This postulate has not yet been confirmed. This special feature makes inorganic–organic nanocages more complex systems than POMs, but also more interesting, as many biological assembly processes also involve hydrophobic interactions and electrostatic interactions.[6]

Herein, we focus on the study of organic–inorganic nanocages of the type $M_{12}L_{24}$ (M = Pd, L = 2,6-bis(4-pyridylethynyl)toluene) in solution. They are novel macromolecules assembled from small building blocks of organic ligands and metal ions. Their shape, size, charge, and composition can be rationally designed by judicious selection of the metal ions and the organic ligands.[7] Such nanocages exist as macrocations in solution and are soluble in polar solvents owing to the charges at the metal centers. The thermodynamic stability, encapsulation, and catalytic properties of $M_{12}L_{24}$ nanocages have been studied in detail.[8] Unlike the M_6L_4 nanocages that we studied previously, which have an octahedral geometry with four open faces, $M_{12}L_{24}$ nanocages possess a cuboctahedral structure with 12 Pd^{II} metal cations (hydrophilic centers) that are evenly distributed on the almost spherical cage surface (Figure 1) and linked by hydrophobic linkers. We previously reported vesicle formation but did not have direct evidence to prove our single-layer model of the large assemblies.[9] Herein, we explore the self-assembly of the $M_{12}L_{24}$ macrocations and compare it with that of other systems. In particular, we use $M_{12}L_{24}$ as a model system to test a new approach to studying the equilibrium between discrete

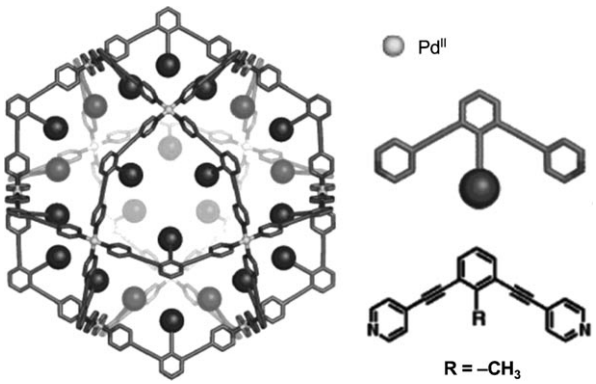

Figure 1. Molecular structure of the $M_{12}L_{24}$ nanocage.

[*] D. Li, Prof. Dr. K. Landskron, Prof. Dr. T. Liu
Department of Chemistry, Lehigh University
Bethlehem, PA 18015 (USA)
E-mail: til204@lehigh.edu
Homepage: http://www.lehigh.edu/~inliu/
Dr. W. Zhou, Prof. Dr. C. J. Kiely
Department of Material Science and Engineering, Lehigh University
Bethlehem, PA 18015 (USA)
Dr. S. Sato, Prof. Dr. M. Fujita
Department of Applied Chemistry, School of Engineering
University of Tokyo
Hongo, Bunkyo-ku, Tokyo 113-8656 (Japan)
E-mail: mfujita@appchem.t.u-tokyo.ac.jp
Homepage: http://fujitalab.t.u-tokyo.ac.jp/index_e/

[**] T.L. gratefully acknowledges support of this research by the NSF (CHE-0545983), the Alfred P. Sloan Foundation, and Lehigh University. We thank Dr. Norm Zheng for his generous help with DOSY NMR spectroscopic characterization.

Supporting information for this article is available on the WWW under http://dx.doi.org/10.1002/anie.201007829.

and aggregated nanocages by NMR spectroscopy. This information is crucial for the interpretation of laser-light-scattering results to obtain the average intercage distance in the assemblies: an important value for our understanding of the nature of the interactions between the macroions.

$M_{12}L_{24}$ nanocages can be readily synthesized in dimethyl sulfoxide (DMSO), acetonitrile, and other polar solvents. Each nanocage cluster carries 24 positive charges balanced by 24 nitrate ions. The nanocages are thermodynamically stable,[8d] and ^{1}H NMR spectroscopic data also confirm that once they have been synthesized in [D_6]DMSO, these nanocages can stay in solution for months without any decomposition or precipitation (see Figure S1 in the Supporting Information). This stability enables us to explore their behavior in solution.

$M_{12}L_{24}$ cationic cages were found to self-assemble into larger structures in [D_6]DMSO, as confirmed by the continuous increase in the total scattered intensity from the solution in static light scattering (SLS) studies and a mode corresponding to large structures in dynamic light scattering (DLS) studies. DLS data (Figure 2) indicated that the large assemblies have narrow size distributions, and their average size (in terms of their hydrodynamic radius (R_h)) did not show an obvious angular dependence (see Figure S2). This latter result suggests that the assemblies have a spherical shape. Meanwhile, the apparent average radius of gyration (R_g) obtained from SLS studies for the large assemblies reveal how the mass of the large assemblies is distributed. A series of solutions of $M_{12}L_{24}$ were prepared by diluting a concentrated solution of $M_{12}L_{24}$ in DMSO (Figure 3d; for the concentrated sample, the molar nanocage/NO_3^- ratio was 1:36). By extrapolating the R_g values to a nanocage concentration of zero, a $R_{g,0}$ value of (38.0 ± 2.0) nm was obtained. This value is very similar to the average $R_{h,0}$ value of (37.8 ± 1.8) nm obtained from DLS measurements. The $R_{g,0}/R_{h,0}$ ratio reflects the shape of the particles in solution, whereby a solid sphere has a value of 0.77, and a hollow sphere has a value close to 1.[5b] Therefore, the relationship $R_{g,0} \approx R_{h,0}$ in this case indicates that the self-assembled large structures are hollow spheres.

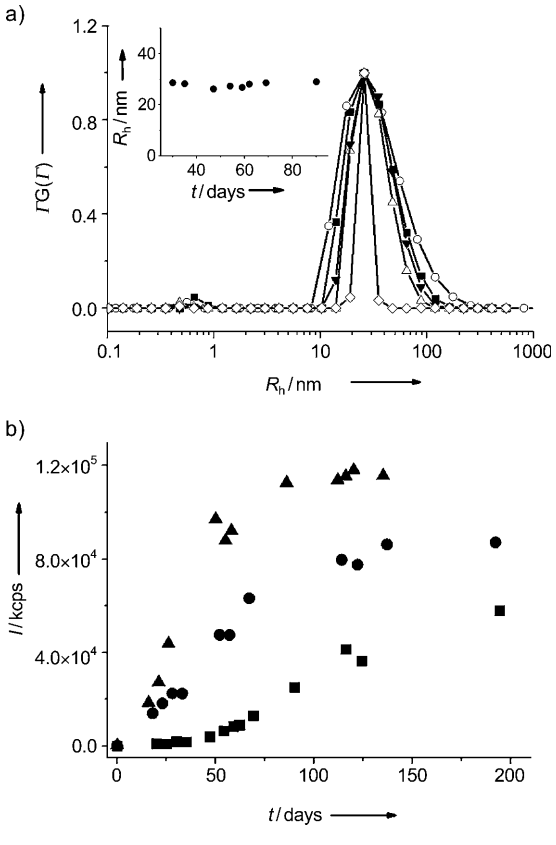

Figure 2. Self-assembly of three $M_{12}L_{24}$-nanocage samples at different NO_3^- concentrations in [D_6]DMSO, as monitored by SLS and DLS. a) Size distribution of the aggregates formed in solution, as calculated by using the software of win CONTIN, with a nanocage/NO_3^- molar ratio of 1:24 (■ day 54, ○ day 59, △ day 62, ▼ day 69, ◇ day 90). The inset shows the average R_h value versus time. b) Total scattered intensity with respect to time for the three samples (■ nanocage/NO_3^- 1:24, ● nanocage/NO_3^- 1:29, ▲ nanocage/NO_3^- 1:36).kcps: kilocounts per second

Time-resolved SLS studies revealed more information about the slow self-assembly of the nanocages into supramolecular structures. In the freshly prepared nanocage solution (with a nanocage/NO_3^- molar ratio of 1:24), very weak scattered intensity was recorded (Figure 2b). This result indicates that the $M_{12}L_{24}$ nanocages initially exist as single cations in solution, as also confirmed by NMR DOSY (diffusion-ordered spectroscopy) analysis (Figure 3a). The total scattered intensity recorded at a scattering angle of 90° from this solution increased slowly with time. Moreover, as shown in the inset in Figure 2a, the size of the large structures (in terms of their R_h value) remained nearly constant during the whole assembly process, which indicates that the structures are quite stable. This observation is consistent with our previous studies on the self-assembly of POM macroanions.[5a,e,10] Therefore, the increase in the scattered intensity with time is mostly due to the increase in the number of assemblies in solution. Since single $M_{12}L_{24}$ nanocages are remarkably stable in DMSO and other polar solvents, the larger structures formed in the current case must be built up from these single nanocage entities. Single free nanocages are always in equilibrium with the large self-assembled structures in solution, as shown by the bimodal size distribution (Figure 2a).

Two-dimensional DOSY ^{1}H NMR spectroscopy is a powerful technique for determining molecular size and measuring molecular interactions on the basis of the self-diffusion coefficient.[11] In a standard DOSY spectrum, the *F*2 domain corresponds to the ^{1}H chemical shift, and the *F*1 domain is the diffusion coefficient for different protons (Figure 3a). The spectrum clearly shows that immediately after their synthesis, the $M_{12}L_{24}$ nanocages remained as monomers; no large structures were observed. From the slope of the linear regression in Figure 3b, the self-diffusion coefficient for a single nanocage was determined to be 5.45×10^{-11} m^{2}s^{-1}, which corresponds to an average R_h value of (1.8 ± 0.3) nm. As the single nanocages progressively formed larger structures in solution, as demonstrated by laser light scattering, the proton signals originating from the nanocage species decreased. An explanation for this observation is that as the single nanocages start to interact with each other to form larger structures, the strong spin–spin interactions of two

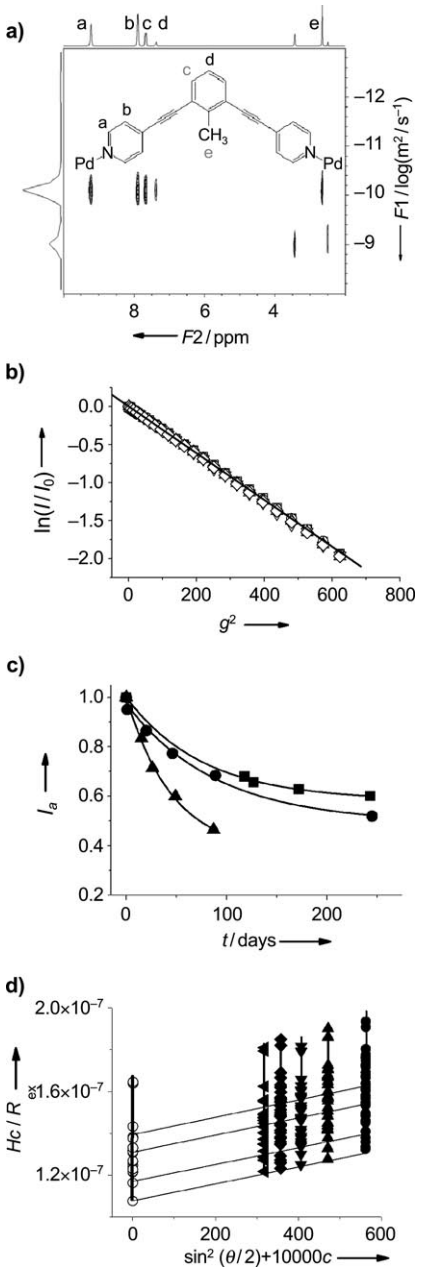

Figure 3. a) Two-dimensional DOSY ^{1}H NMR spectrum of $M_{12}L_{24}$ nanocages in [D_6]DMSO, with a nanocage/NO_3^- ratio of 1:24. b) Normalized nanocage-signal decay as a function of the gradient strength squared (g^2). The measurement was made at 298 K immediately after synthesis of the nanocages. c) ^{1}H NMR signal decay as a function of time for hydrogen atom a of the nanocage. All data points are normalized against the initial intensity at $t = 0$ (■ nanocage/NO_3^- 1:24, ● nanocage/NO_3^- 1:29, ▲ nanocage/NO_3^- 1:36). d) Zimm plot of a series of diluted $M_{12}L_{24}$-nanocage samples in DMSO (-○- extrapolation, ● 5.70 μM, ▲ 4.78 μM, ▼ 4.17 μM, ◆ 3.66 μM, ◀ 3.26 μM). A concentration amendment for large aggregates was made on the basis of the NMR-signal-decay results.

or more neighboring nanocages make the transverse relaxation process so fast that the proton peaks from those nanocages in assemblies become too broad to be detected. A similar proton-signal-decay phenomenon was observed previously during vesicle formation.[12] However, in our current system, the proton-signal decay is rather slow.

If we assume that nanocages only have two states in a dilute solution—they can exist as free monomers and in aggregates—the total proton-signal intensity in ^{1}H NMR spectra will only be from the free monomers. This assumption is reasonable, as we demonstrated earlier that the oligmers (an important intermediate stage for the assembly) have a very limited concentration.[5f] Therefore, when the two states reach equilibrium, the fraction of nanocages that form aggregates can be determined by measuring the decay of the proton-signal intensity. For example, the peak area associated with proton a (integrated from $\delta = 9.00$ to 9.40 ppm) on day 0 was set as the reference value, and relevant measurements made under the same conditions (temperature, probe, receiver gain, number of scans, etc.) on subsequent days were compared to the reference. All three nanocage solutions studied showed a slow but continuous decay of proton-signal intensity (Figure 3c; similar trends were observed when the [D_6]DMSO solvent peak was used as the internal reference). By fitting the data with a first-order exponential decay function, the concentration of nanocage assemblies under equilibrium conditions could be estimated. We found that 41.6% of the total nanocages would form large assemblies at equilibrium when no extra NO_3^- counterions were present.

The above information is especially valuable for calculating the intercage distance on the assembly surface. This distance can be used to judge the nature of the attractive interactions between cationic cages. From the Zimm plot shown in Figure 3d, the weight-averaged molecular weight (M_w) of the large assemblies could be calculated by using the Rayleigh–Gans–Debye equation (see the Supporting Information). The SLS technique favors large particles, and the total scattered intensity in the current SLS measurement was almost exclusively derived from the large particles. From the NMR spectroscopic results, an appropriate correction to the assembly concentration c was made, which resulted in a final M_w value for the large structures of $(9.4 \pm 0.8) \times 10^6\ g\,mol^{-1}$. This value corresponds to 956 ± 81 single nanocages when the molar nanocage/NO_3^- ratio is 1:36.

On the basis of all of the experimental results presented above, we propose a model for this self-assembled structure in solution: a single-layered, hollow, spherical, vesicle-like entity with individual nanocages homogenously distributed on the surface (Figure 4). If we assume that all nanocages are

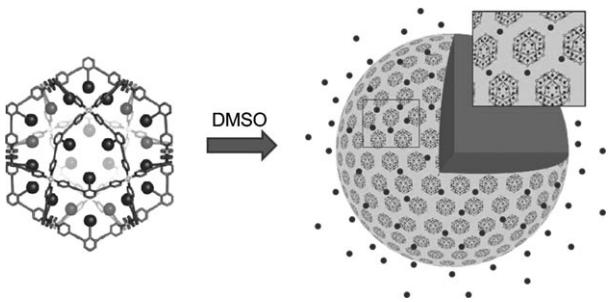

Figure 4. Schematic illustration of the self-assembly of $M_{12}L_{24}$ nanocages in DMSO (small dots are NO_3^- counterions).

arranged with pseudohexagonal close packing, the average center-to-center distance between two adjacent nanocages would be (4.7 ± 0.3) nm. This distance indicates that two adjacent nanocages are very close together but do not touch one another (the diameter of an individual nanocage is approximately 4 nm, as determined by DOSY). We demonstrated previously that the distribution of counterions around macroions plays an important role in holding like-charged macroions together to form blackberry structures. The calculated inter-nanocage distance of (0.7 ± 0.3) nm confirms that counterion-mediated attraction is indeed possible, because there is enough space between the nanocages to accommodate the small counterions (in this case NO_3^-).

More direct evidence for this vesicle-like structure was obtained from (scanning) transmission electron microscopy ((S)TEM) imaging studies (see the Supporting Information for technical details). The vesicle-like structures have a reasonably uniform size (Figure 5a). Some of the vesicle-like structures were found to have shrunk and/or collapsed as a result of evaporation of the solvent from within the hollow structure. However, these collapsed vesicles provided an interesting opportunity to analyze the hollow sphere structure. In the dark square in Figure 5a, a thin single-layer structure of lighter contrast can be seen at the edge of a broken sphere, whereas the other part of the sphere displays a considerably darker contrast level generated by overlap of the top and bottom layers of the vesicle-like structure.

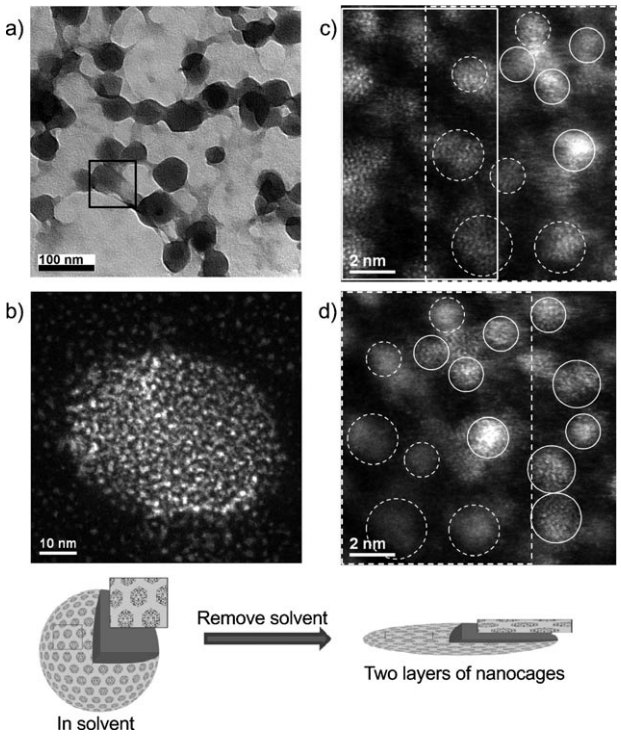

Figure 5. TEM and STEM images of collapsed vesicle-like structures and individual nanocages dispersed on a carbon support film. a) Low-magnification BF images. b) STEM HAADF image of a typical collapsed vesicle-like structure surrounded by an atmosphere of individual nanocages. c,d) STEM HAADF images obtained from a broken edge of a vesicle-like structure at two different focus settings: with the microscope focused on the bottom layer (c) and focused on the top layer (d). For comparative purposes, the white dashed rectangles in the images indicate the exact same area of the sample. The white dashed circles highlight the Pd clusters in the bottom layer, whereas the white solid circles indicate the clusters in the top layer. The white solid rectangle in (c) indicates the broken edge of the vesicle-like structure, where the top layer is gone.

Besides the large vesicle-like structures, individual nanocages were also observed by TEM bright-field (BF) imaging on the basis of mass–thickness contrast. Figure S5 in the Supporting Information shows the random distribution of the free individual nanocages on the carbon film as dark dots. Both the individual nanocages and vesicle-like structures can be better visualized by STEM high-angle annular dark-field (HAADF) imaging with atomic-number (z) contrast information. In Figure 5b, the cluster of Pd atoms associated with each nanocage displays a higher intensity than the dark background of the carbon film owing to the more effective electron scattering by Pd. It is also clear that the vesicle-like structure is formed by the assembly of a large number of nanometer-sized "building blocks": that is, the nanocages. The observed spatial arrangement of individual nanocages in Figure 5b no longer reflects the real structure that would exist in the solution phase, because the vesicle-like structure has deflated and collapsed as a result of the evaporation of solvent from within the structure. However, it is still noticeable from the HAADF images that the individual nanocages in the vesicle-like structure are well-separated, which is consistent with our SLS results.

To further investigate the validity of our proposed monolayer hollow sphere model, we performed through-focal STEM HAADF imaging. Correction of the spherical aberration on our STEM instrument enabled the use of a larger probe-forming aperture, which in turn resulted in a significant reduction in the depth of focus of the images.[13] By systematically changing the focus setting of the microscope lenses, it was then possible to obtain a series of images focused at different depth levels in the sample along the incident-electron-beam direction. The HAADF images shown in Figure 5c,d were obtained from the same general area of a broken edge of a vesicle-like structure at different focus settings. The white dashed rectangles in Figure 5c,d indicate the identical area of the sample. It is clear that when the focus value is changed, different parts of the image go in and out of focus. In fact, all Pd clusters from the nanocages shown in Figure 5c,d can be sorted into two different focus levels, as indicated by the two different types of circles (bold and dashed). This result further confirms our structure model, since a vesicle wall comprised of a single layer of nanocages can be expected to collapse on a flat substrate to give a bilayer of nanocages.

To examine the counterion effect on the self-assembly of the nanocages, we added extra solutions of $Pd(NO_3)_2$ to two freshly prepared nanocage solutions to give the final nanocage/NO_3^- molar ratios 1:29 and 1:36. When a different amount of additional NO_3^- counterions was added, no obvious difference was observed initially in the size of individual nanocages by DOSY. When no additional NO_3^- ions were present in the solution (i.e., no additional counter-anions; the molar nanocage/NO_3^- ratio is then 1:24), the

increase in the scattered intensity with time was much slower than for the other two solutions, and there was a significant lag period (ca. 30 days) before the scattered intensity started to increase significantly (Figure 2b). Furthermore, the kinetic curves for all three samples were sigmoidal, which indicates the existence of a nucleation step followed by a rapid self-association process. As the concentration of NO_3^- ions increased, the lag period before initiation of the self-assembly process became much shorter. Kinetic curves of this type have been observed for many viral-capsid-formation processes and also some polyoxometalate solutions.[1,5f] These observations, taken together with the fact that larger self-assembled structures are formed at higher NO_3^- concentrations (see Figure S3), indicate that the additional NO_3^- counteranions play an important role in the self-assembly of nanocages, most likely by lowering the activation-energy barrier to the formation of the self-assembled structures from individual nanocage macrocations.[6c] More importantly, when extra NO_3^- counterions were added to nanocage solutions, the proton signal decayed much faster (Figure 3c), and the total intensity loss was also more significant (this value increased to 50.8 and 62.6%, respectively, when the nanocage/NO_3^- ratio was 1:29 and 1:36); these results indicate that the presence of additional NO_3^- counterions favors the formation of assemblies.

As noted above, when additional NO_3^- counterions are present in solution, that is, the ionic strength of the solution increases, significantly more nanocages will self-assemble, and the overall size of the vesicle-like structures will also increase. Moreover, when a less polar solvent, such as acetonitrile, was added to the freshly prepared nanocage solutions (the CH_3CN content varied from 20 to 80 vol%), the self-assembly of the nanocages accelerated. At equilibrium, there was a linear relationship between the size of the vesicle-like structures and the inverse dielectric constant of the solvent (Figure 6), which suggests that the size of the structures could be determined by their renormalized charge density.[14] These results all indicate that the counterions play an important role in this self-assembly process, in analogy with the self-assembly of POM macroanions.[10,15] The effective surface charge density of the macroanions is significantly lowered as a result of counterion association, which in turn reduces the repulsion force between two macroanions. In the solution of cationic $M_{12}L_{24}$, we believe that the counterion-mediated attraction is the major driving force for self-assembly.[14] Since each nanocage contains a large portion of aromatic organic ligands, hydrophobic interactions and/or π–π stacking interactions of the organic ligands may also provide additional stabilization to the vesicle-like blackberry structure once it forms. Purely hydrophilic POM clusters have a similar surface charge density to the $M_{12}L_{24}$ nanocages. However, the blackberries formed by POM clusters have an average, roughly estimated interparticle distance of approximately 1.0 nm,[5b,d] whereas the vesicle-like structures formed by $M_{12}L_{24}$ nanocages have a smaller interparticle distance (ca. 0.7 nm), which indicates an additional contribution from other attractive forces, most likely from hydrophobic interactions. A possible scenario is that the existence of the hydrophobic interaction leads to some very close contacts between the nanocages, and these contacts shorten the average intercage distance obtained from SLS measurements.

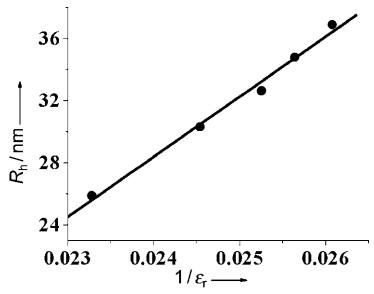

Figure 6. Plot of the average R_h value of the vesicle-like structures in solutions of $M_{12}L_{24}$ nanocages in DMSO mixed with different amounts (40–80 vol%) of CH_3CN against the inverse dielectric constant (ε_r) of the solvent.

The coexistence of electrostatic and hydrophobic interactions makes the self-assembly process of the nanocages remarkably similar to some biological processes, such as viral-capsid formation. Like viral capsids, the vesicle-like structures self-assembled from nanocages are also monolayer spheres with individual nanocages evenly distributed in the wall of the vesicle-like structures. It has also been observed that the viral-capsid-formation process can be accelerated at high salt concentrations.[1,4] In the case of nanocages, the presence of additional salts will also speed up the self-assembly process and induce the formation of larger assemblies. However, the self-assembly of single nanocages into blackberry structures normally requires days or even months to reach equilibrium; in contrast, the time frame for viral-capsid formation is of the order of hours or several days.[1] A possible reason for this difference could be that the specific interaction sites and geometrical restrictions of the viral capsid dimers are missing in our cuboctahedral nanocages. In other words, the degree of freedom of individual nanocages on the surface of the vesicle-like structure is larger than that for protein dimers. The different surface charge density of nanocages and protein dimers may also be an important factor. Furthermore, the viral capsid is a dynamic structure in the sense that its size can vary reversibly in response to different environmental stimuli (i.e. pH value, ionic strength, temperature) by tuning of the dimer–dimer distance and the capsid protein structure.[16] This breathing or swelling mode is quite important in the life cycle of a virus, not only for maintaining the structural integrity of the virus but also for influencing the virus–host interaction and the release of the packaged nucleic acid. The vesicle-like structures formed by nanocages can also "sense" a change in the surrounding conditions (i.e. ionic strength and solvent polarity) and subsequently change their size. These interesting properties of the vesicle-like structures formed by nanocages suggest that the "charge effect" plays an important role in the macroion self-assembly process as well as in viral-capsid formation and stability.

In summary, $M_{12}L_{24}$ nanocages with cuboctahedral symmetry slowly self-assemble into large, monolayered, hollow, spherical vesicle-like blackberry structures in polar solvents. The assembly size can be tuned by adjusting the solvent

polarity or by adding extra electrolytes. Counterion-mediated interactions between nanocages are probably the major driving force for assembly, although hydrophobic interactions and/or π–π stacking interactions of the organic ligands may also contribute to the supramolecular structure. This vesicle-like structure indicates that the self-assembly process is a universal phenomenon for macroions. More importantly, the self-assembly of nanocages shares some remarkable similarities with viral-capsid formation. Indeed, it may be feasible to use such nanocages as model systems to mimic viral capsids. Such studies may possibly lead to a more fundamental understanding of protein–protein interactions.

Experimental Section

The $M_{12}L_{24}$ nanocages were synthesized on the basis of a previously reported procedure[8a] and characterized by ^{1}H NMR spectroscopy. The diluted nanocage samples were prepared by transferring 10–100 μL of the original solution into a clean light-scattering sample cell containing dust-free DMSO (4–5 mL). Stock solutions were diluted prior to the slow self-assembly process in solution. Detailed experimental procedures for DLS/SLS, STEM, and NMR spectroscopy can be found in the Supporting Information.

Received: December 13, 2010
Published online: April 18, 2011

Keywords: interparticle distance · nanocages · self-assembly · vesicles · viral capsids

[1] P. Ceres, A. Zlotnick, *Biochemistry* **2002**, *41*, 11525 – 11531.
[2] A. Zlotnick, *Virology* **2003**, *315*, 269 – 274.
[3] a) K. Matsuura, K. Watanabe, T. Matsuzaki, K. Sakurai, N. Kimizuka, *Angew. Chem.* **2010**, *122*, 9856 – 9859; *Angew. Chem. Int. Ed.* **2010**, *49*, 9662 – 9665; b) L. Cronin, *Angew. Chem.* **2006**, *118*, 3656 – 3658; *Angew. Chem. Int. Ed.* **2006**, *45*, 3576 – 3578; c) A. Müller, D. Rehder, E. T. K. Haupt, A. Merca, H. Bögge, M. Schmidtmann, G. Heinze-Brückner, *Angew. Chem.* **2004**, *116*, 4566 – 4570; *Angew. Chem. Int. Ed.* **2004**, *43*, 4466 – 4470.
[4] W. K. Kegel, P. van der Schoot, *Biophys. J.* **2004**, *86*, 3905 – 3913.
[5] a) T. Liu, *J. Am. Chem. Soc.* **2003**, *125*, 312 – 313; b) T. Liu, E. Diemann, H. Li, A. W. M. Dress, A. Müller, *Nature* **2003**, *426*, 59 – 62; c) G. Liu, Y. Cai, T. Liu, *J. Am. Chem. Soc.* **2004**, *126*, 16690 – 16691; d) G. Liu, T. Liu, *J. Am. Chem. Soc.* **2005**, *127*, 6942 – 6943; e) M. L. Kistler, A. Bhatt, G. Liu, D. Casa, T. Liu, *J. Am. Chem. Soc.* **2007**, *129*, 6453 – 6460; f) J. Zhang, D. Li, G. Liu, K. J. Glover, T. Liu, *J. Am. Chem. Soc.* **2009**, *131*, 15152 – 15159; g) P. P. Mishra, J. Pigga, T. Liu, *J. Am. Chem. Soc.* **2008**, *130*, 1548 – 1549.
[6] a) G. Tresset, W. C. D. Cheong, Y. L. S. Tan, J. Boulaire, Y. M. Lam, *Biophys. J.* **2007**, *93*, 637 – 644; b) D. Baigl, K. Yoshikawa, *Biophys. J.* **2005**, *88*, 3486 – 3493; c) K. S. Schmitz, *J. Phys. Chem. B* **2009**, *113*, 2624 – 2638.
[7] L. Stefan, B. Olenyuk, P. J. Stang, *Chem. Rev.* **2000**, *100*, 853 – 908.
[8] a) M. Tominaga, K. Suzuki, T. Murase, M. Fujita, *J. Am. Chem. Soc.* **2005**, *127*, 11950 – 11951; b) S. Sato, J. Iida, K. Suzuki, M. Kawano, T. Ozeki, M. Fujita, *Science* **2006**, *313*, 1273 – 1276; c) M. Tominaga, K. Suzuki, M. Kawano, T. Kusukawa, T. Ozeki, S. Sakamoto, K. Yamaguchi, M. Fujita, *Angew. Chem.* **2004**, *116*, 5739 – 5743; *Angew. Chem. Int. Ed.* **2004**, *43*, 5621 – 5625; d) S. Sato, Y. Ishido, M. Fujita, *J. Am. Chem. Soc.* **2009**, *131*, 6064 – 6065; e) N. Kamiya, M. Tominaga, S. Sato, M. Fujita, *J. Am. Chem. Soc.* **2007**, *129*, 3816 – 3817; f) K. Suzuki, K. Takao, S. Sato, M. Fujita, *J. Am. Chem. Soc.* **2010**, *132*, 2544 – 2545.
[9] D. Li, J. Zhang, K. Landskron, T. Liu, *J. Am. Chem. Soc.* **2008**, *130*, 4226 – 4227.
[10] G. Liu, M. L. Kistler, T. Li, A. Bhatt, T. Liu, *J. Cluster Sci.* **2006**, *17*, 427 – 443.
[11] Y. Cohen, L. Avram, L. Frish, *Angew. Chem.* **2005**, *117*, 524 – 560; *Angew. Chem. Int. Ed.* **2005**, *44*, 520 – 544.
[12] J. Rodríguez-Hernández, S. Lecommandoux, *J. Am. Chem. Soc.* **2005**, *127*, 2026 – 2027.
[13] A. R. Lupini, A. Y. Borisevich, J. C. Idrobo, H. M. Christen, M. Biegalski, S. J. Pennycook, *Microsc. Microanal.* **2009**, *15*, 441 – 453.
[14] A. A. Verhoeff, M. L. Kistler, A. Bhatt, J. Pigga, T. Liu, W. K. Kegel, *Phys. Rev. Lett.* **2007**, *99*, 066104.
[15] J. M. Pigga, M. L. Kistler, C. Shew, M. R. Antonio, T. Liu, *Angew. Chem.* **2009**, *121*, 6660 – 6664; *Angew. Chem. Int. Ed.* **2009**, *48*, 6538 – 6542.
[16] a) J. B. Bancroft, G. J. Hills, R. Markham, *Virology* **1967**, *31*, 354 – 379; b) L. S. Ehrlich, T. Liu, S. Scarlata, B. Chu, C. A. Carter, *Biophys. J.* **2001**, *81*, 586 – 594; c) B. Jacrot, *J. Mol. Biol.* **1975**, *95*, 433 – 446; d) G. Vriend, M. A. Hemminga, B. J. M. Verduin, T. J. Schaafsma, *FEBS Lett.* **1982**, *146*, 319 – 321.

